Organic Electrolytes Doped ZnO Layer as the Electron Transport Layer for Bulk Heterojunction Polymer Solar Cells

*Youn Hwan Kim, Dong Geun Kim, Ratna Dewi Maduwu, Ho Cheol Jin, Doo Kyung Moon, and Joo Hyun Kim**

ZnO layers doped with small molecule viologen derivatives, i.e., 1,1′-bis(4-hydroxypropyl)-[4,4′-bipyridine]-1,1′-diium bromide (V—OH) or 1,1′-bis(2,3-dihydroxypropyl)-[4,4′-bipyridine]-1,1′-diium bromide (V—2OH), are prepared and used as the electron transport layer in inverted polymer solar cells (iPSCs). The presence of V—OH (or V—2OH) in ZnO layer and the formation of homogeneous V—OH (or V—2OH) doped ZnO layer are confirmed by X-ray photoelectron spectroscopy. The electron mobilities of doped ZnO layers are comparable to those of pristine ZnO because the crystallinity of the ZnO layer is not significantly affected by the doping process. Kelvin probe microscopy measurements show that the work function of doped ZnO layers is in the range of −4.2 – −4.3 eV, which is higher than that of pristine ZnO (−4.5 eV). This is due to the formation of interface dipoles at the interface between the ZnO layer and the active layer. The water contact angle data reflect the existence of quaternary ammonium bromide on the surface, and unreacted hydroxyl groups are pointed away from the surface of the ZnO layer. iPSCs based on V—OH doped ZnO and V—2OH doped ZnO exhibit power conversion efficiencies (PCEs) up to 9.0% and 8.6%, which are dramatically enhanced compared to the device based on pristine ZnO (PCE = 7.4%).

1. Introduction

Polymer solar cells (PSCs) have widely attracted attention because of their advantages, such as low fabrication cost, large area application, and fabrication of flexible devices.[1–4] There has been rapid improvement in the power conversion efficiencies (PCEs) of PSCs. Recently 10% or more of PCEs have been reported. Such values have been achieved due to tremendous accomplishments being made in the development of efficient conjugated materials including polymers and oligomers[5–7] and electrode interface engineering.[8]

Recently, inverted type PSCs have been focused because they have better stability than devices using the conventional architecture.[9,10] A ZnO layer prepared by a sol-gel process is widely used as the electron transport layer between the ITO cathode and the active layer.[11] For inverted PSCs, one of the important factors for achieving the high PCE is facile electron collection at the interface between the ZnO layer and the active layer. Reducing the energy gap at the interface and passivation of ZnO surface are important to improve the performances of the devices. Many approaches have been tried to modify the surface of ZnO such as deposition of thin layer of conjugated or non-conjugated polyelectrolytes[12–21] (i.e., interlayer), metal chelates,[22] and self-assembled monolayer (SAM)[23–26] treatments on the top of the ZnO surface to improve electron collection at the ZnO surface. In case of the former method, the performance of the device is very sensitive to the thickness of the interlayer, which is normally in the range of 5–10 nm and should be optimized. However, it is very difficult to control the interlayer thickness in the range of 5–10 nm using the large area fabrication systems seen in practical applications, such as slot die casting or spray coating processes. Therefore, an alternative method, which avoids the need for fine control of interlayer thickness, is to blend materials, such as poly(ethyleneoxide),[23] polyethyleneimine,[24] and C60 derivatives[25] into ZnO matrix. Devices with such blended ZnO layer showed enhanced performance. However, the electron mobilities of such blended ZnO layer were decreased because of intrinsically insulating nature of the materials. To overcome this problem, blends of ZnO with materials such as 1,2-ethandithiol[26] and ethylenediaminetetraacetic acid (EDTA)[27] have been used as the electron transporting layers.

We have reported the synthesis of 1′-bis(4-hydroxypropyl)- [4,4′-bipyridine]-1,1′-diium bromide (V—OH)[19] and 1,1′-bis(2,3-dihydroxypropyl)-[4,4′-bipyridine]-1,1′-diium bromide (V—2OH)[28] (shown in **Figure 1**) and their application in inverted PSCs as

Y. H. Kim, D. G. Kim, R. D. Maduwu, H. C. Jin, Prof. J. H. Kim
Department of Polymer Engineering
Pukyong National University
Busan 48547, Korea
E-mail: jkim@pknu.ac.kr

Prof. D. K. Moon
Department of Materials Chemistry and Engineering
Konkuk University
Seoul 05029, Korea

DOI: 10.1002/solr.201800086

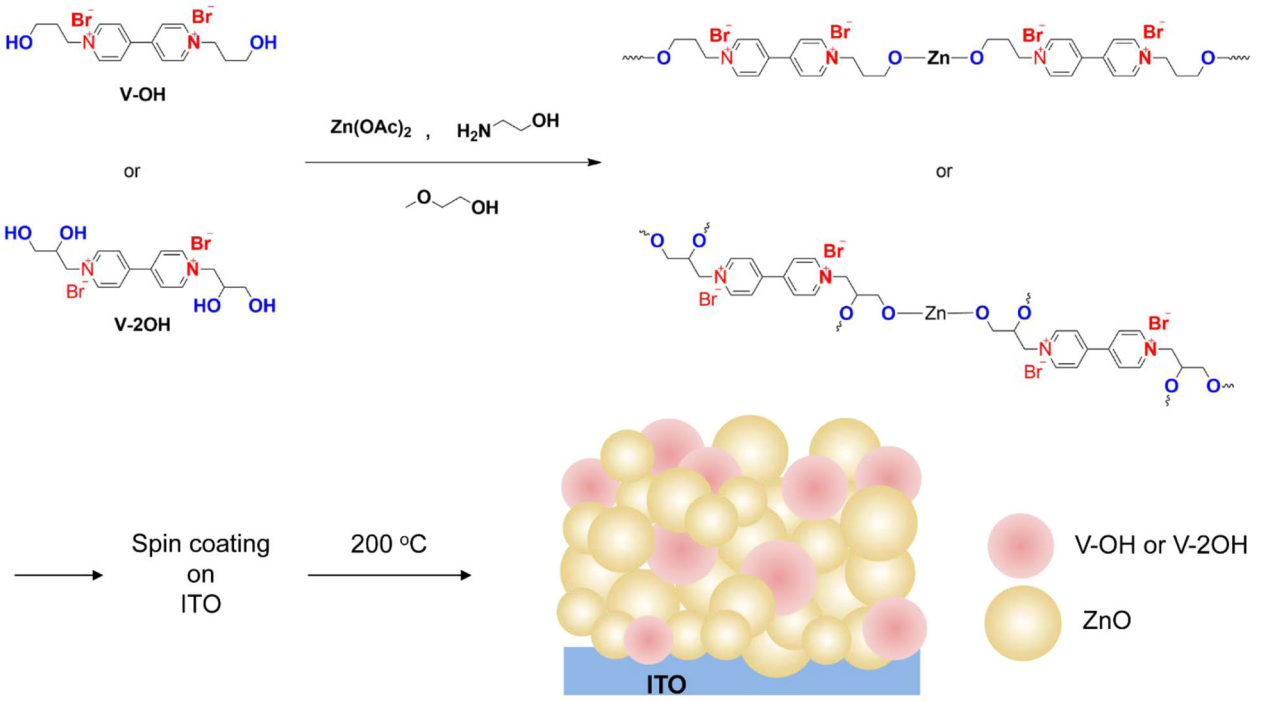

Figure 1. Chemical structure of V—OH and V—2OH and schematic illustration of preparation of V—OH (or V—2OH) doped ZnO layer.

the cathode buffer layer. Viologen derivatives are well known materials for cathode buffer layer in the PSCs[13,14,29,30] because of their several advantages such as low lying LUMO level due to high electron affinity and good solubility in protic solvent. In this report, we prepare V—OH (or V—2OH) doped ZnO layer as the electron transporting layer and apply it to inverted type PSCs to enhance the performances of the device without sacrificing the electron mobility. As illustrated in Figure 1, both V—OH and V—2OH doped ZnO layer can be obtained by a sol-gel process. Homogeneous ZnO layer with V—OH and V—2OH as dopants is produced due to multiple hydroxyl (—OH) groups in V—OH and V—2OH. V—OH (or V—2OH) doping into the ZnO matrix improves the PCE from 7.4% (short circuit current (J_{sc}) = 14.2 mA cm^{-2}, open circuit voltage (V_{oc}) = 0.76 V, fill factor (FF) = 66.6%) based on pristine ZnO to 9.0% (J_{sc} = 17.3 mA cm^{-2}, V_{oc} = 0.74 V, FF = 70.0%) based on V—OH doped ZnO and 8.6% (J_{sc} = 17.2 mA cm^{-2}, V_{oc} = 0.73 V, FF = 68.9%) based on V—2OH doped ZnO, respectively, without sacrificing the electron mobility of the ZnO layer. Improvement in the PCE of the devices results from the enhanced J_{sc}. This is due to the improvement in the electron collection capability from the active layer to the electron transport layer by reducing the energy barrier at the interface, i.e., transition from a Schottky to an Ohmic contact.

2. Results and Discussion

2.1. Photovoltaic Properties

We employed V—OH or V—2OH doped ZnO layer as the electron transport layer in inverted BHJ polymer solar cells (PSCs) with structure of ITO/V—OH (or V—2OH) doped ZnO/PTB7:$PC_{71}BM$(1:1.5)/MoO_3/Ag (as shown in **Figure 2**a) to investigate the effect of V—OH (or V—2OH) on the photovoltaic properties. We prepared the V—OH (or V—2OH) doped ZnO through a sol-gel process. A precursor solution was prepared by adding different weight ratios of V—OH (or V—2OH) (0.0, 1.0, 2.0, and 3.0 wt%) to the zinc acetate dihydrates to optimize the concentration of V—OH (or V—2OH). Details are described in the Supporting Information. Figure 2b represent the energy level diagram of the materials used in the device and current density–voltage curves of PSCs under illumination (inset: under the dark condition), respectively. Thermogravimetric analysis (TGA) of V—OH and V—2OH at a heating rate of 10 °C min^{-1} under the air atmosphere were carried out, and the results are shown in Figure S1, Supporting Information. According to the TGA thermograms, V—OH and V—2OH showed good thermal stability up to 270 °C. The point of 5% weight loss (T_d) of V—OH and V—2OH appeared at 271 and 274 °C, respectively, in the TGA thermograms.

As shown in Figure 2c and **Table 1**, the J_{sc} and FF of the devices with V—OH (or V—2OH) are increased, while the V_{oc} data are slightly decreased. Among the V—OH doped devices tested, the 2.0 wt% V—OH doped device showed the highest PCE of 9.0% (J_{sc} = 17.3 mA cm^{-2}, V_{oc} = 0.74 V, FF = 70.0%), which is dramatically enhanced over the device without dopant. Note, the best PCE of the device with 2.0 wt% of V—OH mainly resulted from the J_{sc} enhancement. The work function of V—OH (or V—2OH) doped ZnO were measured by Kelvin probe microscopy (KPM). As shown in Figure 1b, the work function data of V-OH (or V—2OH) doped ZnO and undoped ZnO were −4.2 – −4.3 eV and −4.5 eV, respectively. The dopant concentration does not critically affect the work function of V—OH (or V—2OH) doped ZnO. However, the work function of doped ZnO layers are

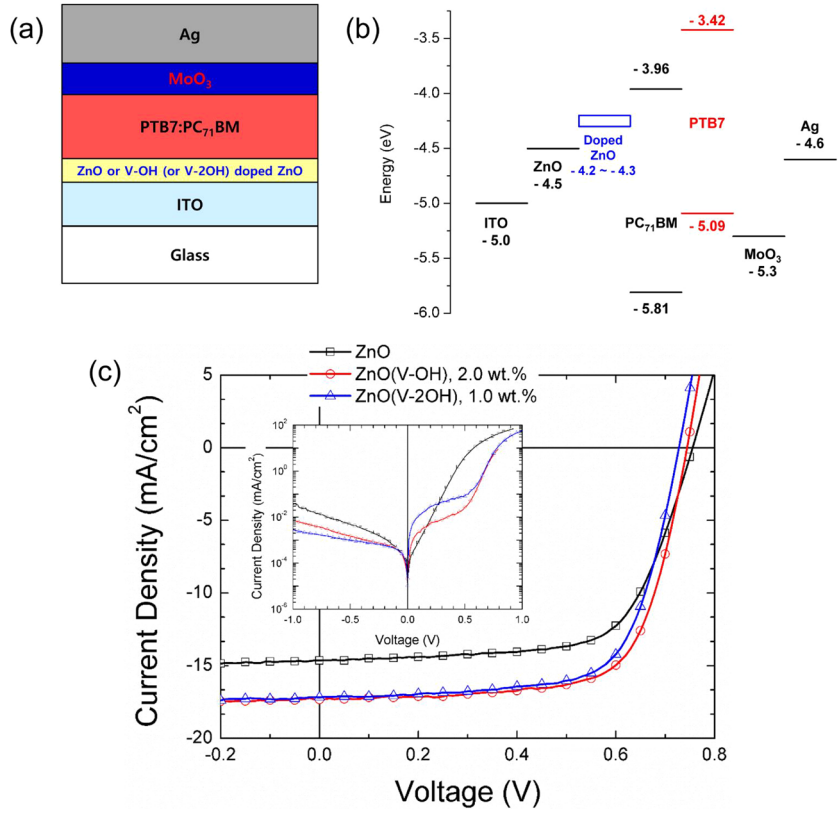

Figure 2. a) Device structures, b) energy level diagram of materials in the research, and c) current density–voltage curves of PSCs under illumination (inset: in the dark condition).

higher than that of pristine ZnO. It should be noted that the J_{sc} result is strongly related to the work function of the ZnO layer. Charge collection behavior is interrupted by a large Schottky barrier height at the electrode interfaces. Thus, Ohmic contact at the electrode interface is a crucial factor to get high J_{sc}. Thus, the J_{sc} enhancement is strongly correlated with the change in the work function of the ZnO layer. As for V—2OH doped devices, the device based on 1.0 wt% doped ZnO showed the best performances (PCE = 8.6%, $J_{sc} = 17.2\,mA\,cm^{-2}$, $V_{oc} = 0.73\,V$, FF = 68.9%). The results in the devices based on V—2OH exhibited very similar features in the devices based on V—OH. The concentration of V—2OH to ZnO precursor is exactly half of the concentration of V—OH to ZnO precursor. This is due to the fact that the number of hydroxyl groups in V—2OH is exactly twice the number of hydroxyl groups in V—OH. In general, the work function difference in the charge transporting layer is not main factor affecting the built-in potential and V_{oc} in case of Fermi-level pinning.[31] This is due to that the V_{oc} of the device based on V—OH and V—2OH doped ZnO is almost identical to that of the device with pristine ZnO. As shown in J—V curves under the dark condition (inset of Figure 2c), the leakage current of the device based V—OH (or V—2OH) doped ZnO is lower than that of the device based on ZnO owing to the recombination of charges is suppressed.[32,33] The series resistance (R_s) of the device was estimated by the inverse slope near high current regime in the dark current density-voltage curves (inset of Figure 2c). The R_s data also well correlated with the performances of the devices. Incident photon-to-current efficiency (IPCE) curves (Figure S2, Supporting Information) showed very good agreement with the J_{sc} data of the devices.

To measure the electron mobility of pristine and doped ZnO, we fabricated the electron-only devices as shown in the inset of **Figure 3**a, electron mobility of the device was estimated by the space-charge-limited current (SCLC) method and calculated using Mott-Gurney equation.[34,35] As shown in Figure 3a, above built-in voltage, the current density and electric field shows a characteristics of SCLC. The electron mobility of the device with optimum concentration of 2.0 wt% V—OH doped ZnO was $1.06 \times 10^{-3}\,cm^2\,V^{-1}\,s^{-1}$, which are comparable to electron mobility of V—2OH ($0.88 \times 10^{-3}\,cm^2\,V^{-1}\,s^{-1}$). In addition, both values are very similar to that of the device based on pristine ZnO ($0.76 \times 10^{-4}\,cm^2\,V^{-1}\,s^{-1}$). It suggested the fact that the structural ordering of pristine ZnO is

Table 1. The performances of PSCs showing the best PCE. The averages and deviations (20 devices are averaged) are summarized in parentheses.

ETL	wt% [mol%]	J_{sc} [mA cm^{-2}]	V_{oc} [V]	FF [%]	PCE [%]	R_s[a)] [Ω cm^2]	Calculated J_{sc} [mA cm^{-2}][b)]
ZnO	0%	14.7 (14.4 ± 0.2)	0.76 (0.76 ± 0.01)	66.6 (67.8 ± 1.15)	7.4 (7.3 ± 0.1)	9.6	14.9
ZnO (V—OH)	1.0% (0.15%)	15.2 (15.0 ± 0.1)	0.75 (0.74 ± 0.01)	72.0 (72.1 ± 0.41)	8.2 (8.1 ± 0.1)	3.4	–
	2.0% (0.31%)	17.3 (17.0 ± 0.3)	0.74 (0.74 ± 0.01)	70.0 (70.1 ± 0.40)	9.0 (8.7 ± 0.1)	3.2	16.8
	3.0% (0.46%)	15.3 (15.1 ± 0.2)	0.74 (0.74 ± 0.01)	71.5 (71.1 ± 0.45)	8.1 (8.0 ± 0.1)	3.8	–
ZnO (V—2OH)	1.0% (0.14%)	17.2 (16.6 ± 0.3)	0.73 (0.73 ± 0.01)	68.9 (70.0 ± 0.48)	8.6 (8.5 ± 0.1)	3.2	16.5
	2.0% (0.29%)	15.1 (15.0 ± 0.1)	0.74 (0.74 ± 0.01)	70.5 (70.4 ± 0.05)	7.9 (7.8 ± 0.1)	3.3	–
	3.0% (0.43%)	15.7 (15.5 ± 0.2)	0.74 (0.74 ± 0.01)	70.0 (70.1 ± 0.14)	8.1 (8.0 ± 0.1)	3.3	–

[a)] Series resistance are calculated from the device showing the best PCE; b) Calculated from the IPCE curves; the performance data of the device based on 0.5 wt% V—2OH doped ZnO are shown in Figure S4.

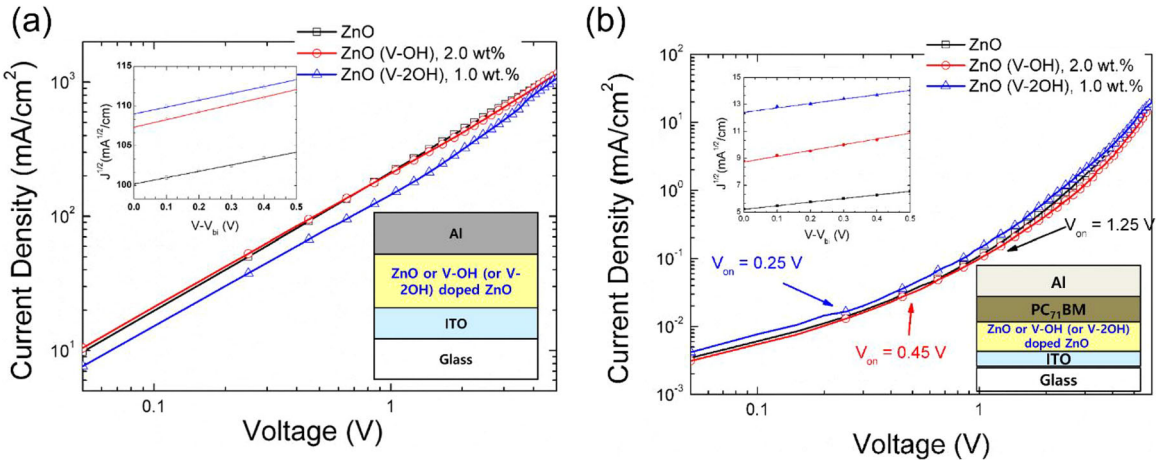

Figure 3. Current density—voltage curves of electron-only devices, with fitted line (*V*, applied voltage; V_{bi}, built-in voltage). See the insets for the different device structure.

almost same as the structural ordering of doped ZnO. Doping of organic electrolytes in the research improves the PCE of the device without sacrificing the electron mobility of ZnO layer.

To study further the effect of doping on the property change of ZnO layer, electron-only devices with the structure of ITO/ZnO or doped ZnO/$PC_{71}BM$/Al were fabricated (inset Figure 3b). As shown in Figure 3b, the current density and voltage relationship shows a characteristics of SCLC. The electron mobilities of the devices based on V—OH and V—2OH were $4.75 \times 10^{-4}\,cm^2\,V^{-1}\,s^{-1}$, and $2.77 \times 10^{-4}\,cm^2\,V^{-1}\,s^{-1}$, respectively. The order of magnitude of those value are same as the value based on pristine ZnO ($1.85 \times 10^{-4}\,cm^2\,V^{-1}\,s^{-1}$). However, the turn-on voltage (estimated

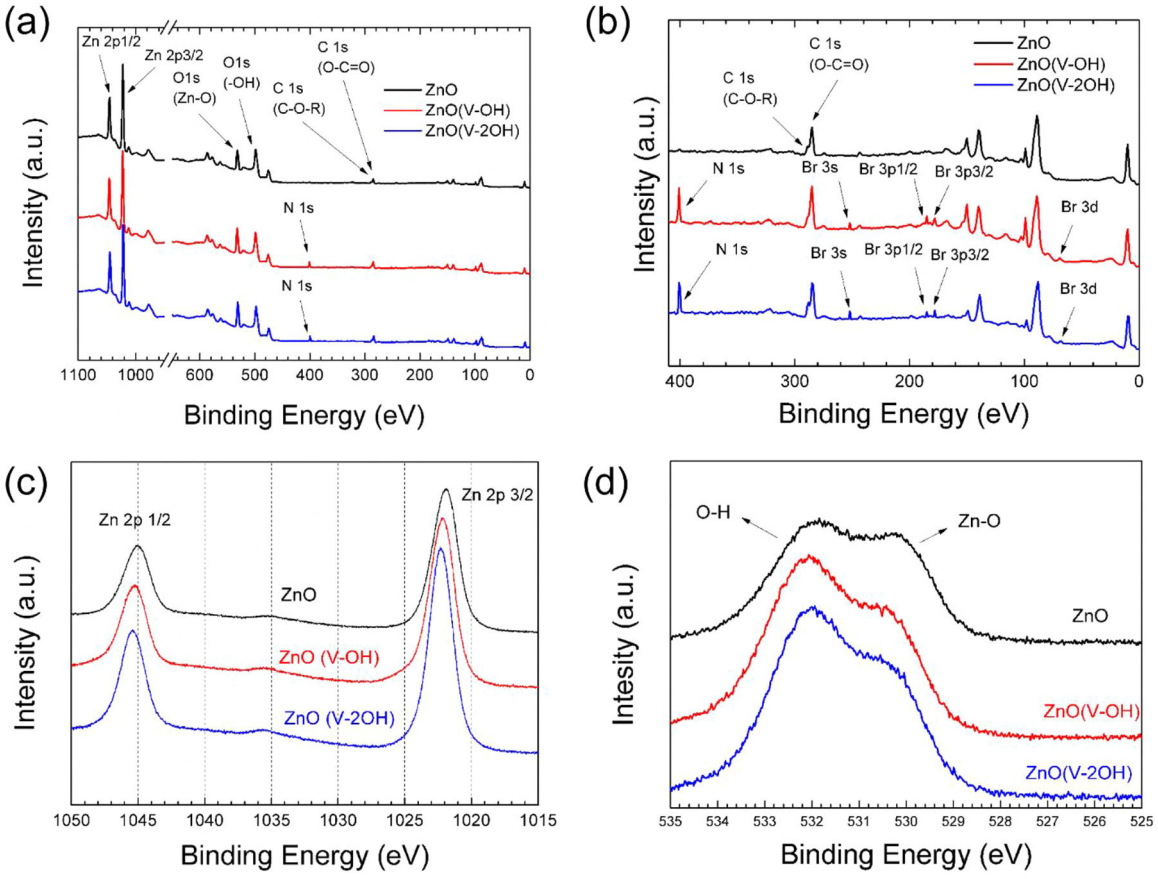

Figure 4. a, b) XPS survey spectra, c) Zn 2p, and d) O 1s spectra of ZnO, 2.0 wt% V—OH doped ZnO, and 1.0 wt% V—2OH doped ZnO, respectively.

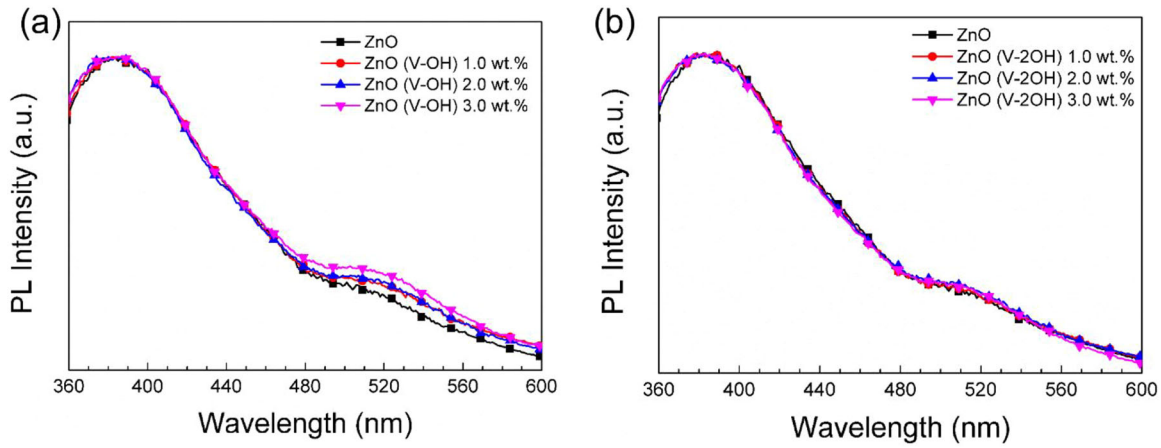

Figure 5. Normalized photoluminescence spectra of ZnO, V—OH doped ZnO, and V—2OH doped ZnO (excited at 325 nm).

according to the literature[36]) of the device based on V—OH and V—2OH were 0.25 and 0.45 V, respectively, which are significantly smaller than that of the device based on pristine ZnO (1.25 V). This means that the electron injection process from doped ZnO layer to $PC_{71}BM$ layer is much easier than pristine ZnO layer to PCBM layer, owing to the energy gap between the ZnO layer and the $PC_{71}BM$ layer is reduced by doping of V—OH and V—OH. The results are very well correlated with the improvement of J_{sc} by V—OH and V—2OH doping in ZnO layer. The device were kept in a nitrogen atmosphere without passivation. The PCE of devices with ZnO, V—OH doped ZnO, and V—2OH doped ZnO showed 78.5%, 89.8%, and 89.4%, respectively, of its initial PCE. One notice that the V—OH and V—2OH are able to have the better stability of the performance of the devices.

2.2. Characterization of V—OH and V—2OH doped ZnO

In order to survey the existence of V—OH and V—2OH in the ZnO layer, we performed X-ray photoelectron spectroscopy (XPS). The survey spectra of pristine ZnO, 2.0 wt% V—OH doped ZnO and 1.0wt% V—2OH doped ZnO are showed in

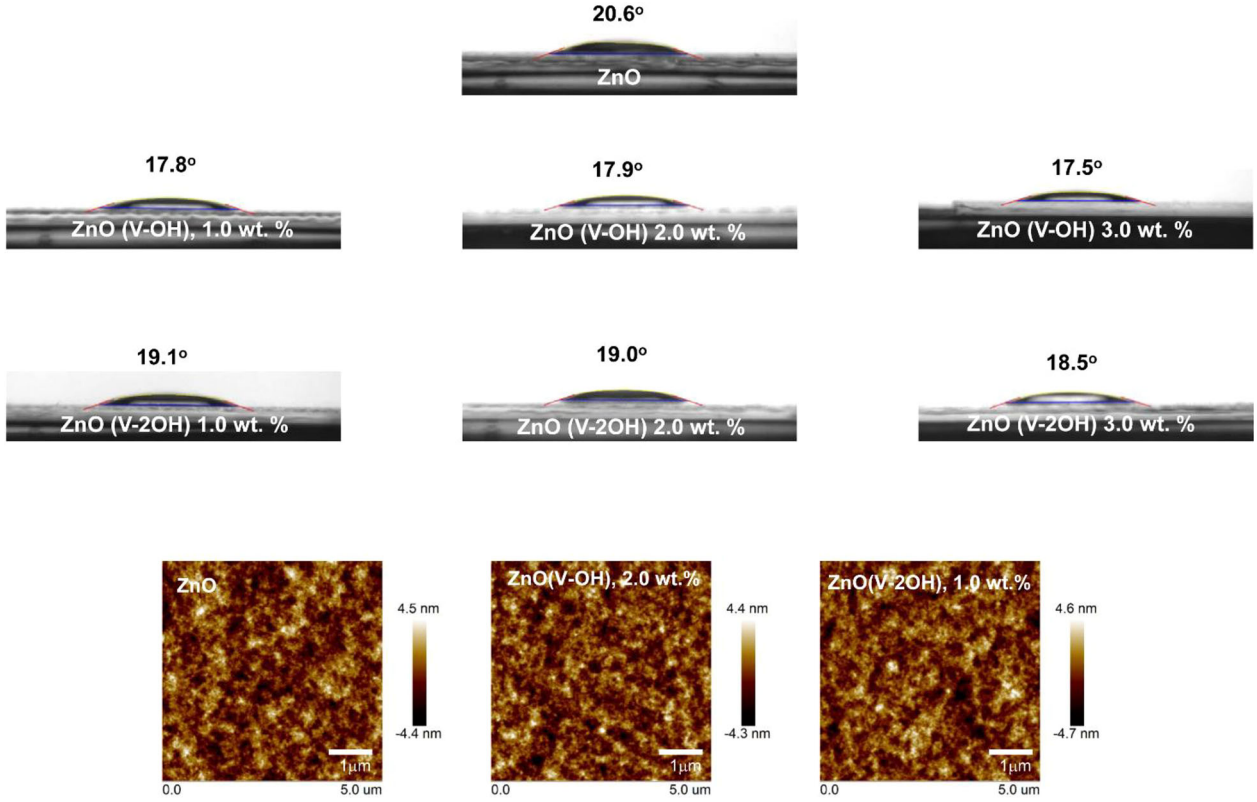

Figure 6. Static water contact angle data and AFM images of ZnO, V—OH doped ZnO, and V—2OH doped ZnO.

Figure 4a,b. As shown in Figure 4a,b, V—OH (or V—2OH) doped in the ZnO layer shows characteristic peaks of nitrogen and bromide at binding energies (BEs) of 401, 252, 185, 178, and 65 eV, which correspond to N1s, Br3d, Br3p3/2, Br3p1/2, and Br3s, respectively. In the survey spectrum of pristine ZnO, no peaks from nitrogen and bromide appeared. BEs of 1045 and 1021 eV in pristine ZnO are assigned to the Zn 2p1/2 and Zn 2p3/2, respectively.[12] The position of BE of Zn peaks in V—OH (or V—2OH) doped ZnO are moved toward higher BE energy.[37,38] This is due to the change in surroundings of the Zn atoms, which has become more electron rich compared to pristine ZnO. The more electron rich state near the Zn atoms is coincident with the formation of chemical bonding between Zn and V—OH (or V—2OH).

As shown in the XPS spectrum of pristine ZnO (Figure 3d), peaks at BE of 532 and 530 eV correspond to oxygen ion on −OH and ZnO, respectively. Peak intensity ratios between O—H and Zn—O of V—OH doped ZnO and V—2OH doped ZnO were higher than that of pristine ZnO. Apparently, the number of defect sites in V—OH (or V—2OH) doped ZnO layer are greater than those of pristine ZnO. However, one should notice that peak intensity at BE of 532 eV might be originated from both the oxygen defect in ZnO and free −OH in V—OH (or V—2OH). Thus, we cannot directly estimate the number of defect sites based on the XPS results. To investigate the existence of defect sites in ZnO layer, we measured photoluminescence (PL) spectra of the ZnO layers. As shown in **Figure 5**, the ZnO layers were excited at 325 nm. The emission band at 383 nm corresponds to the band-edge emission. In addition, very weak emission band at 510 nm is observed, which is attributed to the defect sites. As for V—OH, the intensity of emission band at 510 nm in V—OH doped ZnO is slightly higher than that of pristine ZnO. For V—OH doped ZnO, defect emission in doped ZnO layer is almost identical to that of pristine ZnO. One can notice that doping process does not affect the generation of defect sites. Intensity of X-ray diffraction (XRD) patterns (see Figure S3, Supporting Information) of ZnO, V—OH doped ZnO, and V—2OH doped ZnO film showed relatively weak characteristics because annealing temperature was relatively low (200 °C). However, intensity of the peaks from V—OH (or V—2OH) doped ZnO is comparable to those of the pristine ZnO film. This means that the addition of V—OH (or V—2OH) up to 3.0 wt% does not significantly affect the crystallinity of ZnO. We investigated the static water contact angle (SWCA) and the surface morphology to investigate the surface properties of the ZnO layer. As shown in **Figure 6**, SWCA of the surface of V—OH (or V—2OH) doped ZnO was smaller than that of the pristine ZnO surface. The surface of V—OH (or V—2OH) doped ZnO is more hydrophilic than that of ZnO surface owing to the unreacted free —OH groups in V—OH or V—2OH. The results are very consistent with the PL results. Surface topographic images of doped ZnO surface are almost identical to that of ZnO. The surface roughness of the ZnO, V—OH doped ZnO, and V—2OH doped ZnO surface are 1.04, 0.99, and 1.05 nm, respectively. The properties of the ZnO surface do not seem to be crucial factor for the performances of the devices.

3. Conclusion

Small molecular viologen derivatives (V—OH and V—2OH) doped ZnO has been successfully prepared. A ZnO layer with V—OH (or V—2OH) as a dopant improves the PCE from 7.4% ($J_{sc} = 14.2$ mA cm^{-2}, $V_{oc} = 0.76$ V, FF = 66.6%) based on pristine ZnO to 9.0% ($J_{sc} = 17.3$ mA cm^{-2}, $V_{oc} = 0.74$ V, FF = 70.0%) based on V—OH and 8.6% ($J_{sc} = 17.2$ mA cm^{-2}, $V_{oc} = 0.73$ V, FF = 68.9%) based on V—2OH, respectively, without sacrificing the electron mobility of the ZnO layer. Improvement in the PCE of the devices resulted from the J_{sc} improvement. This is due to the fact that the electron collection ability from the active layer to the electron transport layer is improved by reducing the energy barrier at the interface.

Supporting Information

Experimental details including materials, synthesis, measurements, and fabrication of devices, TGA, J—V curves of the device based on 0.5 wt% V—2OH doped ZnO, IPCE, and XRD data are available in supporting information. Supporting Information is available from the Wiley Online Library or from the author.

Acknowledgements

This research work was supported by the New and Renewable Energy Core Technology Program of the Korea Institute of Energy Technology Evaluation and Planning (KETEP) granted financial resource from the Ministry of Trade, Industry and Energy, Republic of Korea (20153010140030) and Basic Science Research Program through the National Research Foundation of Korea (NRF) funded by the Ministry of Education, Science and Technology (201603930154). Y.H. Kim and D.G. Kim contributed equally to this work.

Conflict of Interest

The authors declare no conflict of interest.

Keywords

doping, electrolyte, inverted polymer solar cells, viologen

Received: March 26, 2018
Revised: May 14, 2018
Published online:

[1] G. Yu, J. Gao, J. C. Hummelen, F. Wudl, A. J. Heeger, *Science* **1995**, *270*, 1789.
[2] S. Gunes, H. Neugebauer, N. S. Sariciftci, *Chem. Rev.* **2007**, *107*, 1324.
[3] L. Lu, T. Zheng, Q. Wu, A. M. Schneider, D. Zhao, L. Yu, *Chem. Rev.* **2015**, *115*, 12666.
[4] Y.-W. Su, S.-C. Lan, K.-H. Wei, *Mater. Today* **2012**, *15*, 554.
[5] V. Vohra, K. Kawashima, T. Kakara, T. Koganezawa, I. Osaka, K. Takimiya, H. Murata, *Nat. Photonics* **2015**, *9*, 403.
[6] H.-J. Song, D.-H. Kim, E.-J. Lee, J. R. Hwa, D.- K. Moon, *Sol. Energy Mater. Sol. Cells* **2014**, *123*, 112.

[7] J. Zhao, Y. Li, G. Yang, K. Jiang, H. Lin, H. Ade, W. Ma, H. Yan, *Nat. Energy* **2016**, *1*, 15027.
[8] S. H. Oh, S. I. Na, J. Jo, B. Lim, D. Vak, D. Y. Kim, *Adv. Funct. Mater.* **2010**, *20*, 1977.
[9] S. Nho, G. Baek, S. Park, B. R. Lee, M. J. Cha, D. C. Lim, J. H. Seo, S.-H. Oh, M. H. Song, S. Cho, *Energy Environ. Sci.* **2016**, *9*, 240.
[10] Y. Sun, J. H. Seo, C. J. Takacs, J. Seifter, A. J. Heeger, *Adv. Mater.* **2011**, *23*, 1679.
[11] C. E. Small, S. Chen, J. Subbiah, C. M. Amb, S.-W. Tsang, T.-H. Lai, J. R. Reynolds, F. So, *Nat. Photon.* **2012**, *6*, 115.
[12] M. Y. Jo, Y. E. Ha, J. H. Kim, *Sol. Energy Mater. Sol. Cells* **2012**, *107*, 1.
[13] M. Y. Jo, Y. E. Ha, J. H. Kim, *Org. Electron.* **2013**, *14*, 995.
[14] G. E. Lim, Y. E. Ha, M. Y. Jo, J. Park, Y. C. Kang, J. H. Kim, *ACS Appl. Mater. Interfaces* **2013**, *5*, 6508.
[15] Y. E. Ha, G. E. Lim, M. Y. Jo, J. Park, Y. C. Kang, S. J. Moon, J. H. Kim, *J. Mater. Chem. C* **2004**, *2*, 3820.
[16] W. Xu, Z. Kan, T. Ye, L. Zhao, W.-Y. Lai, R. Xia, G. Lanzani, P. E. Keivanidis, W. Huang, *ACS Appl. Mater. Interfaces* **2015**, *7*, 452.
[17] Y. H. Kim, N. Sylvianti, M. A. Marsya, J. Park, Y.- C. Kang, D. K. Moon, J. H. Kim, *ACS Appl. Mater. Interfaces* **2016**, *8*, 32992.
[18] Y. H. Kim, N. Sylvianti, M. A. Marsya, D. K. Moon, J. H. Kim, *Org. Electron.* **2016**, *39*, 163.
[19] T. T. Do, H. S. Hong, Y. E. Ha, S. I. Yoo, Y. S. Won, M.-J. Moon, J. H. Kim, *Macromol. Res.* **2015**, *23*, 367.
[20] J. P. Han, E. J. Lee, Y. W. Han, T. H. Lee, D. K. Moon, *J. Ind. Eng. Chem.* **2017**, *45*, 44.
[21] H.-K. Lin, Y.-W. Su, H.-C. Chen, Y.-J. Huang, K.-H. Wei, *ACS Appl. Mater. Interfaces* **2016**, *8*, 24603.
[22] S.-Y. Chang, Y.-C. Lin, P. Sun, Y.-T. Hsieh, L. Meng, S.-H. Bae, Y.-W. Su, W Huang, C. Zhu, G. Li, K.-H. Wei, Y. Yang, *Solar RRL* **2017**, *1*, 1700139.
[23] S. Shao, K. Zheng, T. N. Pullerits, F. Zhang, *ACS Appl. Mater. Interfaces* **2013**, *5*, 380.
[24] H.-C. Chen, S.-W. Lin, J.-M. Jiang, Y.- W. Su, K.-H. Wei, *ACS Appl. Mater. Interfaces* **2015**, *7*, 6273.
[25] S.-H. Liao, H.-J. Jhuo, Y.-C. Cheng, S.-A. Chen, *Adv. Mater.* **2013**, *25*, 4766.
[26] H. Yang, T. Wu, T. Hu, X. Hu, L. Chen, Y. Chen, *J. Mater. Chem. C* **2016**, *4*, 8783.
[27] X. Li, X. Liu, W. Zhang, H.-Q. Wang, J. Fang, *Chem. Mater.* **2017**, *29*, 4176.
[28] Y. H. Kim, D. G. Kim, J. H. Kim, *Appl. Chem. Eng.* **2016**, *27*, 512.
[29] T. T. Do, H. S. Hong, Y. E. Ha, J. Park, Y.-C. Kang, J. H. Kim, *ACS Appl. Mater. Interfaces* **2015**, *7*, 3335.
[30] T. T. Do, H. S. Hong, Y. E. Ha, C.-Y. Park, J. H. Kim, *Macromol. Res.* **2015**, *23*, 177.
[31] E. L. Ratcliff, B. Zacher, N. R. Armstrong, *J. Phys. Chem. Lett.* **2011**, *2*, 1337.
[32] T. Yang, M. Wang, C. Duan, X. Hu, L. Huang, J. Peng, F. Huang, X. Gong, *Energy Environ. Sci.* **2012**, *5*, 8208.
[33] X. Gong, M. Tong, F. G. Brunetti, J. Seo, Y. Sun, D. Moses, F. Wudl, A. J. Heeger, *Adv. Mater.* **2011**, *23*, 2272.
[34] Y. Wang, Y. Liu, S. Chen, R. Peng, Z. Ge, *Chem. Mater.* **2013**, *25*, 3196.
[35] S. Guo, B. Cao, W. Wang, J.-F. Moulin, P. Muller-Buschbaum, *ACS Appl. Mater. Interfaces* **2015**, *7*, 4641.
[36] I. D. Parker, *J. Appl. Phys.* **1994**, *75*, 1656.
[37] D. Gao, J. Zhang, G. Yang, J. Zhang, Z. Shi, J. Qi, Z. Zhang, D. Xue, *J. Phys. Chem. C* **2010**, *114*, 13477.
[38] S. H. Liao, H. J. Jhuo, Y. S. Cheng, S. A. Chen, *Adv. Mater.* **2013**, *25*, 4766.